J. Fluid Mech. (1972), *vol.* 52, *part* 4, *pp.* 753–780
Printed in Great Britain

On generalized-vortex boundary layers

By R. J. BELCHER,† O. R. BURGGRAF AND K. STEWARTSON‡

Department of Aeronautical and Astronautical Engineering,
The Ohio State University

(Received 20 September 1971)

We define a generalized vortex to have azimuthal velocity proportional to a power of radius r^{-n}. The properties of the steady laminar boundary layer generated by such a vortex over a fixed coaxial disk of radius a are examined. Though the boundary-layer thickness is zero at the edge of the disk, reversals of the radial component of velocity u must occur, so that an extra boundary condition is needed at any interior boundary radius r_E to make the structure unique. Numerical integrations of the unsteady governing equations were carried out for $n = -1$, 0, $\frac{1}{2}$ and 1. When $n = 0$ and -1 solutions of the self-similar equations are known for an infinite disk. Assuming terminal similarity to fix the boundary conditions at $r = r_E$ when $u_r > 0$, a consistent solution was found which agrees with those of the self-similar equations when r_E is small. However, if $n = \frac{1}{2}$ and 1, no similarity solutions are known, although the terminal structure for $n = 1$ was deduced earlier by the present authors. From the numerical integration for $n = \frac{1}{2}$, we are able to deduce the limit structure for $r \to 0$ by using a combination of analytic and numerical techniques with the proviso of a consistent self-similar form as $r_E \to 0$. The structure is then analogous to a ladder consisting of an infinite number of regions where viscosity may be neglected, each separated by much thinner viscous transitional regions playing the role of the rungs. This structure appears to be characteristic of all generalized vortices for which $0{\cdot}1217 < n < 1$.

1. Introduction

A generalized vortex is a circulatory motion in which the azimuthal velocity V is a function of r, the distance from the axis of rotation. Simple examples are $V \propto r$, corresponding to rigid-body rotation and $V \propto r^{-1}$, corresponding to a potential vortex. More general forms are common, for example, in the atmosphere and in vortex chambers. We shall be particularly interested here in flows in which $V \propto r^{-n}$ where n is a constant. Such forms have been suggested as approximate fits of observed velocity distributions; thus Riehl (1954) reports that values of n between 0·4 and 0·6 are appropriate to hurricanes. Generalized vortices have attracted most interest in the past, however, because of the interesting properties of their associated boundary layers.

† Present address: Vought Aeronautics Company, P.O. Box 5907, Dallas, Texas 75222.
‡ Present address: Department of Mathematics, University College, London, Gower Street, London, W.C.1.

Suppose that the vortex is set up above a fixed impermeable plane $z = 0$ perpendicular to the axis of rotation. As shown by Rott & Lewellen (1966), the equations governing the boundary layer near $z = 0$ may be formally reduced to a set of ordinary differential equations in which the azimuthal velocity V is of the form $r^{-n} g^*(\eta)$, where $\eta = z/r^{\frac{1}{2}(1+n)}$ and the radial velocity u is of the form $r^{-n} f^*(\eta)$. The solution properties of the equations satisfied by f^*, g^* have been the subject of much study. For $n = -1$ (rigid-body rotation), Bödewadt (1940) determined the numerical properties of f^* and g^*, and Mcleod (1971) showed rigorously that solutions do exist. On the other hand, Goldshtik (1960) also showed rigorously that, when the Navier–Stokes equations are used for $n = +1$ (the potential vortex), the corresponding equations have a solution only when the Reynolds number is small; Serrin (1972) was able to generalize the study by including another parameter in the equations, thereby obtaining new formal solutions for all Reynolds numbers. However, their physical significance as $r \to \infty$ is not yet clear. King & Lewellen (1964) carried out an extensive numerical program aimed at integrating the similarity equations for $n > -1$ and were able, in spite of considerable difficulties, to obtain acceptable solutions if $0 \geqslant n \geqslant -1$. As n increases toward zero, the structure of these solutions becomes more and more bizarre, velocity overshoots of as much as 60 % being reported and the boundary-layer thickness increasing with great rapidity. They ascribed their inability to obtain solutions for $n > 0{\cdot}1$ to numerical difficulties and stated that solutions are possible for all $n < 1$.

We are not aware of any successful attempts to extend appreciably the range over which numerical solutions can be found, although Kuo (1971) reports a numerical solution for $n = 0{\cdot}04$. On the other hand, Olsen (private communication) reports that he is unable to obtain a solution if $n \sim 0{\cdot}5$. It seems likely that the non-existence when $n = 1$ is not isolated; instead there is a number $n_0 < 1$, such that solutions exist if $n < n_0$ and do not exist if $n > n_0$. The present study supports this view very strongly, and we propose that in fact

$$n_0 = 0{\cdot}1217.$$

Another reason for studying these vortex boundary layers is that they throw further light on the behaviour of boundary layers, under a fluid in general circulatory motion, commonly occurring in practice. Even though the surface near which the boundary layer occurs is plane, it must be of finite extent, so that self-similar solutions, if they exist, can at best be relevant only to those parts of the plane remote from the edge. Further, in all the self-similar solutions computed, the radial velocity changes sign repeatedly as η increases, so that the solution can be regarded neither as strictly an initial velocity profile nor as a terminating velocity profile. One might take an extreme point of view, and ask whether similarity solutions have a role to play in the structure of boundary layers on finite planes even if they exist, and, if they do not exist, what can be said about the structure, particularly near $r = 0$. The only other known case of non-existent self-similar solutions in fluid mechanics occurs with the Falkner–Skan equations, and the physical meaning to be attached is that separation has

occurred at an earlier stage in the development of the boundary layer. For the vortex problem, however, the pressure gradient is favourable.

The Kármán rotating disk is an obvious example of a solution to the boundary-layer equations that is relevant to a finite plane, and it is of course also a self-similar solution. It is relevant to the finite problem because the radial flow is everywhere outward, so that edge effects cannot penetrate inward. For $n = +1$ (the potential vortex), the radial flow is everywhere inward, so that the boundary-layer equations for steady flow can be solved by forward integration from the edge of the disk inward. Burggraf, Stewartson & Belcher (1971) carried out such a calculation down to radii less than 5 % of the disk radius, which was sufficiently close to the axis to allow a coherent description of the terminal boundary layer, even though no similarity solution exists for this case. It was found instead that the boundary layer divides itself up into two parts when r is small. There is an inner region of thickness $\delta \propto r$ in which viscous effects are important but the azimuthal velocity is relatively negligible. This part of the boundary layer has a self-similar character and at the outer edge the radial velocity is equal to the azimuthal velocity in the potential vortex. Outside this part the flow is largely inviscid, the radial velocity falls to zero, the azimuthal velocity rises to its free-stream value and the particular shape of the velocity profiles depends on the previous history of the boundary layer. The numerical integration was started from the edge and advanced inward using a step-by-step method, and was successful because the radial velocity does not change sign anywhere in the flow field.

In the present paper the aim is to develop a comparable body of knowledge about the boundary layer when $|n| \leqslant 1$. To this end, four values of n ($-1, 0, 0{\cdot}5, 1$) were considered, and a new method of integration developed to determine the flow field. It has already been mentioned that all solutions for $n < 1$ show sign reversals in the radial velocity; this means that forward integration from the edge of the disk should become unstable. The similarity solutions in particular exhibit these sign reversals. Now it proves impractical, even when $n = 1$, to compute the solution right up to $r = 0$. We therefore considered the possibility of obtaining solutions for $1 \geqslant r \geqslant r_E$, where r_E is sufficiently small that the structure of the terminal solution as $r \to 0$ can be inferred from knowledge of the solution near r_E. But a solution in $1 \geqslant r \geqslant r_E$ is not uniquely determined by the conditions on the disk, in the free stream and at the edge of the disk, since we can apply arbitrary conditions on that part of the line $r = r_E$ where $u > 0$. Physically, the reason is that small disturbances travel parallel to the disk with the local velocity, and hence move outwards if $u > 0$ and inwards if $u < 0$. They also diffuse across the boundary layer, of course. A change in the boundary condition at $r = r_E$, at a point where $u < 0$, causes a disturbance which immediately travels outside the region of interest, and is therefore irrelevant, but a change, at a point where $u > 0$, travels into the region of interest and modifies the flow there. A fuller discussion of this cause of non-uniqueness is given by Brown & Stewartson (1969).

The numerical study of parabolic equations with boundary conditions imposed at two longitudinal stations is still in its infancy, and to our knowledge only one successful solution has been published. This is by Hall (1969), who considered the

impulsive motion of a flat plate, the governing equations being reducible to a problem of this sort. A complete solution was obtained by attacking the original unsteady two-dimensional problem and regarding time as an integration strip. Here we follow Hall by introducing time as an additional variable, and carrying the integration forward in time until the solution is substantially steady. This criterion is not always easy to enforce for the solution may change slowly with time, but nevertheless evolve into a different structure over a long period, as Pearson (1965) has noted. Our results are subject to this problem; nevertheless, we can draw a fairly complete picture as to the terminal structure of the flow.

Clearly some conditions must be imposed at $r = r_E$, and we choose them as follows. To permit the terminal boundary layer to evolve as a similarity solution (when it exists), the equations of motion can be written in terms of the variable

$$\tilde{Z} = z/r^{\tilde{\beta}}, \tag{1.1}$$

where $\tilde{\beta} = \frac{1}{2}(n+1)$ for the conventional similarity solutions. Then, at those points on the line $r = r_E$ at which $u > 0$, we require

$$\frac{\partial}{\partial r}(r^n u) = \frac{\partial}{\partial r}(r^n v) = 0, \tag{1.2}$$

where these derivatives are evaluated on the line $\tilde{Z}$ = constant. Since condition (1.2) is consistent with similarity solutions regardless of the size of u, it also provides a test for whether or not such solutions exist. For, if (1.2) is not even approximately satisfied on $r = r_E$ when $u < 0$ and r_E is small, then a self-similar limit of the form assumed is not being approached as $r_E \to 0$. It was found that for $n = -1$ and $n = 0$, with $\tilde{\beta}$ given as above, consistent numerical results were obtained, closely approaching the known similarity solutions. However, to obtain consistent numerical results for $n = 0{\cdot}5$, it was necessary to alter the value of $\tilde{\beta}$ as suggested by our analysis of § 7.

2. Equations of motion

Let r^*, θ, z^* be a set of cylindrical polar co-ordinates with r^* measuring distance from the z^* axis. Suppose that the fluid occupies all of space except for a fixed finite plane defined by $z^* = 0$, $0 < r^* < a$. The velocity of the fluid at almost all points of space, but specifically not in the neighbourhood of the plane, is circulatory with

$$u^* = 0, \quad v^* = V^*(r^*), \quad w^* = 0, \tag{2.1}$$

where u^*, v^*, w^* are the velocity components in the r^*, θ, z^* directions respectively. The fluid satisfies the no-slip condition on the plane so that

$$u^* = v^* = w^* = 0 \quad \text{at} \quad z^* = 0, \quad r^* < a. \tag{2.2}$$

We wish to study the boundary layer induced by this vortex in the neighbourhood of the plane, and for this we make the additional assumption that it is initiated at the outside edge $r^* = a$ and grows inwards. The subsequent study of the boundary layer is consistent with this hypothesis. The usual boundary-layer arguments

then show that the pressure is constant across the layer of thickness δ, and that

$$\delta \sim a\left(\frac{\nu}{aV^*(a)}\right)^{\frac{1}{2}}.$$

In fact, writing

$$\left.\begin{aligned} r = r^*/a, \quad z = z^*\left(\frac{V^*(a)}{a\nu}\right)^{\frac{1}{2}}, \quad u = u^*/V^*(a), \\ v = v^*/V^*(a), \quad w = w^*\left(\frac{a}{\nu V^*(a)}\right)^{\frac{1}{2}}, \quad V(r) = V^*/V^*(a), \end{aligned}\right\} \tag{2.3}$$

the momentum equations governing the motion in the boundary layer reduce to

$$u\frac{\partial u}{\partial r} + w\frac{\partial u}{\partial z} - \frac{v^2}{r} = -\frac{V^2}{r} + \frac{\partial^2 u}{\partial z^2}, \tag{2.4}$$

and

$$u\frac{\partial v}{\partial r} + w\frac{\partial v}{\partial z} + \frac{uv}{r} = \frac{\partial^2 v}{\partial z^2}. \tag{2.5}$$

The equation of continuity may conveniently be written in terms of a stream function ψ, i.e.

$$u = \frac{1}{r}\frac{\partial \psi}{\partial z}, \quad w = -\frac{1}{r}\frac{\partial \psi}{\partial r}. \tag{2.6}$$

The boundary conditions available to us are

$$\psi = u = v = w = 0 \quad \text{at} \quad z = 0, \quad r < 1, \tag{2.7}$$

$$u = 0, \quad v = 1 \quad \text{at} \quad r = 1, \quad z > 0, \tag{2.8}$$

and

$$u \to 0, \quad v \to V(r) \quad \text{as} \quad z \to \infty, \quad r < 1, \tag{2.9}$$

but we shall find that these are not sufficient to specify the solution completely. If the integration is terminated at $r = r_E$, then we must also assign values to u and v at all points of the line $r = r_E$ at which $u > 0$.

In this paper we shall usually take $V = r^{-n}$.

3. The structure as $z \to \infty$, and as $r \to 1-$

For fixed $r < 1$, we can expect that w approaches a finite limit $W(r)$ as $z \to \infty$, from the equation of continuity, and this is confirmed both from the numerical studies and from the asymptotic structure of the solution, which we shall now investigate. We write

$$u = \tilde{u}, \quad v = V(r) + \tilde{v}, \quad w = W(r) + \tilde{w}, \tag{3.1}$$

substitute into the governing equations, and neglect squares and products of all tilda quantities. This is justified when z is sufficiently large provided the limits, as $z \to \infty$, are approached smoothly. Then $\tilde{u}$ and $\tilde{v}$ satisfy

$$\left.\begin{aligned} W\frac{\partial \tilde{u}}{\partial z} - \frac{2V}{r}\tilde{v} = \frac{\partial^2 \tilde{u}}{\partial z^2}, \\ W\frac{\partial \tilde{v}}{\partial z} + \tilde{u}\left(\frac{dV}{dr} + \frac{V}{r}\right) = \frac{\partial^2 \tilde{v}}{\partial z^2}. \end{aligned}\right\} \tag{3.2}$$

Clearly $\tilde{u}$ and $\tilde{v}$ depend exponentially on z and so we write

$$\tilde{u} = A(r)\exp\{sz\}, \quad \tilde{v} = B(r)\exp\{sz\}, \tag{3.3}$$

where A, B, s are functions of r to be found. On substituting these expressions into (3.2), we find that such a solution is possible only if

$$(s^2 - Ws)^2 + \frac{2V}{r^2}\frac{d}{dr}(rV) = 0, \tag{3.4}$$

and then

$$\frac{2V}{r}B + (s^2 - Ws)A = 0. \tag{3.5}$$

It follows immediately from (3.4) that, if

$$\frac{d}{dr}(r^2V^2) > 0, \tag{3.6}$$

i.e. if the square of the circulation increases with radius, then s must be complex, so that u and v both oscillate about zero with an amplitude which diminishes exponentially. It is interesting to note that this criterion is the same as that of Rayleigh (1916) for the stability of a fluid motion to inviscid disturbance. For the swirling flow of special interest here $V = r^{-n}$, and so

$$s^2 - Ws = \pm i[2(1-n)]^{\frac{1}{2}} r^{-(1+n)}, \quad \text{if} \quad n < 1. \tag{3.7}$$

Thus, it is possible to find two values of s such that $\mathrm{Re}\, s < 0$. For $n = 1$, there is only one acceptable solution $s = W$ and the A and B are independent. Therefore, if $n = 1$ we can expect that $W < 0$, and so it proved in the numerical study.

With $n < 1$ the behaviour of u and v as $z \to \infty$ is oscillatory for all $r < 1$. This seems to be at variance with the initial structure of the boundary layer at $r = 1-$ given by Stewartson (1958), who showed that the structure of the solution near $r = 1$ is of the form

$$\left.\begin{aligned} u &= (1-r)^{\frac{1}{2}}\mathscr{F}(\sigma), \quad v = \mathscr{G}(\sigma), \\ w &= (1-r)^{-\frac{1}{4}}[\tfrac{3}{4}\mathscr{F} - \tfrac{1}{4}\sigma\mathscr{F}'], \end{aligned}\right\} \tag{3.8}$$

where

$$\sigma = z/(1-r)^{\frac{1}{4}}, \tag{3.9}$$

and the primes denote differentiation with respect to σ.

Here $\mathscr{F}$ and $\mathscr{G}$ satisfy

$$\mathscr{F}''' - \tfrac{3}{4}\mathscr{F}\mathscr{F}'' + \tfrac{1}{2}\mathscr{F}'^2 = 1 - \mathscr{G}^2, \quad \mathscr{G}'' - \tfrac{3}{4}\mathscr{F}\mathscr{G}' = 0, \tag{3.10}$$

with boundary conditions

$$\mathscr{F}(0) = \mathscr{F}'(0) = \mathscr{G}(0) = 0, \quad \mathscr{F}'(\infty) = 0, \quad \mathscr{G}(\infty) = 1. \tag{3.11}$$

The relative errors in (3.8) are $O(1-r)$, and a formal expansion can indeed be set up in integer powers of $(1-r)$, the coefficients of which are functions of σ that can be determined seriatim.

It can be shown from (3.10) that $\mathscr{G}'$ has only one sign, which is in apparent contradiction to (3.7) and (3.3). A resolution can be obtained on noting that, according to (3.8),

$$w \sim \tfrac{3}{4}(1-r)^{-\frac{1}{4}}\mathscr{F}(\infty) \quad \text{when} \quad \sigma \gg 1, \quad (1-r) \ll 1. \tag{3.12}$$

If $\mathscr{F}(\infty) > 0$, (3.10) could have no solutions satisfying $\mathscr{G}(\infty) = 1$, $\mathscr{G}(0) = 0$, whence in (3.7) W must be large and negative. We then have, for $r \to 1$,

$$s = W \pm \frac{i}{W}(2-2n)^{\frac{1}{2}} + \ldots,$$

and

$$u \sim \frac{2C\exp\{Wz\}}{[2(1-n)]^{\frac{1}{2}}}\sin\left\{\frac{z}{W}[2(1-n)]^{\frac{1}{2}} + \delta\right\} + \ldots, \tag{3.13a}$$

$$v \sim 1 - C\exp\{Wz\}\cos\left\{\frac{z}{W}[2(1-n)]^{\frac{1}{2}} + \delta\right\} + \ldots, \tag{3.13b}$$

when $|1-r| \ll 1$; here C and δ are functions of r to be found. A match between (3.13) when $z \ll |W|$ and the solution of (3.10) when $\sigma \gg 1$ now follows easily if we make the additional assumption, verified subsequently, that $|\delta| \ll 1$. For then (3.13) tells us that

$$u \approx C\exp\{Wz\}\left[\frac{\delta}{[2(1-n)]^{\frac{1}{2}}} + \frac{z}{W}\right], \quad v \approx 1 - C\exp\{Wz\} \tag{3.14}$$

when $z \ll W$. On the other hand, from (3.10), when $\sigma \gg 1$

$$\mathscr{G} \approx 1 - E_1\exp\{3\sigma\mathscr{F}(\infty)/4\}, \quad \mathscr{F}' \approx \left[E_2 + \frac{8E_1\sigma}{3\mathscr{F}(\infty)}\right]\exp\{3\sigma\mathscr{F}(\infty)/4\}, \tag{3.15}$$

where, using Mack's (1962) accurate solution of (3.10),

$$E_1 = 4{\cdot}46, \quad E_2 = 8{\cdot}20.$$

On expressing σ in terms of the variables z and $(1-r)$, and comparing with (3.14), we see that

$$C = E_1, \quad \delta = \frac{E_2}{2E_1}[2(1-n)(1-r)]^{\frac{1}{2}}, \tag{3.16}$$

and the match is complete. Summarizing, when $z \gg (1-r)^{\frac{1}{4}}$ and $(1-r) \ll 1$,

$$\left.\begin{aligned} u &\sim \frac{2E_1}{[2(1-n)]^{\frac{1}{2}}}\exp\{3\sigma\mathscr{F}(\infty)/4\}\sin\left[\left(\frac{4\sigma}{3\mathscr{F}(\infty)} + \frac{E_2}{2E_1}\right)[2(1-r)(1-n)]^{\frac{1}{2}}\right], \\ v &\sim 1 - E_1\exp\{3\sigma\mathscr{F}(\infty)/4\}\cos\left[\left(\frac{4\sigma}{3\mathscr{F}(\infty)} + \frac{E_2}{2E_1}\right)[2(1-r)(1-n)]^{\frac{1}{2}}\right]. \end{aligned}\right\} \tag{3.17}$$

Thus, the oscillations in the radial velocity component are present in a rudimentary form in the initial profile at $r = 1$, although for small values of $(1-r)$ they occur at distances from the plane $\sim (1-r)^{-\frac{1}{4}}$, and the magnitudes are exponentially small. From a numerical point of view, the presence of these oscillations means that, as posed in (2.4)–(2.9), the boundary-value problem does not have a unique solution for any $r < 1$, and additional information must be supplied to ensure uniqueness.

4. The numerical computations†

The sign reversals in the radial velocity, analysed in § 3, not only imply non-uniqueness, but also ensure that a valid numerical procedure for solving the boundary-value problem (2.4)–(2.9), by marching in the radial direction, will

† The emphasis here and in § 5 is on the steady-state results. Additional information on the time-dependent numerical results is given by Belcher (1970).

utimately become unstable. Cooke (1966) and Anderson (1966) both attempted such a calculation for $n = -1$ by forward integration from the edge of the disk inward. Cooke's method operated satisfactorily down to 75 % of the disk radius, but failed to converge to a unique result for smaller radii. On the other hand, Anderson's procedure functioned down to 40 % of the disk radius, at which point the results agreed closely with King & Lewellen's (1964) solution of the Bödewadt problem. Anderson's success is surprising, since both non-uniqueness and instability would be expected, owing to the appearance of regions of radial outflow. Consequently, it was decided to use the time-dependent approach here.

In setting up the numerical procedure, variables were selected that had been shown to accentuate the relevant details of the flow for $n = 1$. Thus a composite 'similarity' variable ζ was introduced in place of z, defined as

$$\zeta = z r^{-\frac{1}{2}(1+n)}(1-r)^{-\frac{1}{4}}, \tag{4.1a}$$

where the factor $(1-r)^{-\frac{1}{4}}$ effects the proper similarity behaviour near $r = 1$, (3.9), and the factor $r^{-\frac{1}{2}(1+n)}$ is the scaling appropriate to any local flow structure, near $r = 0$, that might develop independent of conditions at the edge $r = 1$. The importance of a gradual approach to the axis has been demonstrated for the potential vortex. This was accomplished by introducing a new radial variable

$$\xi = -\log r, \tag{4.1b}$$

so that the edge of the disk now appears at $\xi = 0$, and the centre is pushed off exponentially to $\xi \to \infty$. The velocity components u, v, w are scaled accordingly, as

$$\left.\begin{aligned} ur^n &= (1-e^{-\xi})^{\frac{1}{2}} f(\xi, \zeta, \tau), \\ vr^n &= g(\xi, \zeta, \tau), \\ wr^{\frac{1}{2}(1+n)} &= (1-e^{-\xi})^{-\frac{1}{4}} h(\xi, \zeta, \tau), \end{aligned}\right\} \tag{4.2}$$

where τ is a non-dimensional time,

$$\tau = t^* V^*(a)/a.$$

In these new variables, the equations of motion (2.4), (2.5) take the form

$$\left.\begin{aligned} &[\exp\{-(1+n)\xi\}(1-\exp(-\xi))^{\frac{1}{2}}]\frac{\partial f}{\partial \tau} \\ &\quad = \frac{\partial^2 f}{\partial \zeta^2} - \left[h - \left(\frac{1+n}{2} - \frac{3+2n}{4}\exp(-\xi)\right)\zeta f\right]\frac{\partial f}{\partial \zeta} \\ &\qquad + (1-\exp(-\xi))f\frac{\partial f}{\partial \xi} + \left(n + \frac{1-2n}{2}\exp(-\xi)\right)f^2 - 1 + g^2, \\ &[\exp\{-(1+n)\xi\}(1-\exp(-\xi))^{\frac{1}{2}}]\frac{\partial g}{\partial \tau} \\ &\quad = \frac{\partial^2 g}{\partial \zeta^2} - \left[h - \left(\frac{1+n}{2} - \frac{3+2n}{4}\exp(-\xi)\right)\zeta f\right]\frac{\partial g}{\partial \zeta} \\ &\qquad + (1-\exp(-\xi))f\frac{\partial g}{\partial \xi} - (1-n)(1-\exp(-\xi))fg, \\ &\frac{\partial h}{\partial \zeta} = \left(\frac{1+n}{2} - \frac{3+2n}{4}\exp(-\xi)\right)\zeta\frac{\partial f}{\partial \zeta} \\ &\qquad + (1-\exp(-\xi))\frac{\partial f}{\partial \xi} + \left[1-n-\left(\frac{3-2n}{2}\right)\exp(-\xi)\right]f. \end{aligned}\right\} \tag{4.3}$$

The form of the similarity equations for the edge of the disk result by setting $\xi = 0$, and those for the axis by letting $\xi \to \infty$.

For $\xi \to 0$, (4.3) indicates that the time derivatives are singular; i.e. the steady-state solution is established immediately at the edge of this disk. Consequently, Stewartson's (1958) profiles were applied as boundary and initial conditions for $\xi = 0$, $\tau \geqslant 0$. For $\xi > 0$, the no-slip condition (2.7) was applied at $\zeta = 0$, and the inviscid vortex given by (2.9) was required at ζ_∞ for $\tau > 0$, where ζ_∞ is the value of ζ at the outer edge of the mesh. For $\tau = 0$, this outer-edge condition was applied right down to the disk, corresponding to 'switching on' the viscosity at $\tau = 0$. Finally, at the innermost radial station $\xi = \xi_E$, the boundary condition (1.2) was applied at points for which f is positive, as discussed in § 1. In effect this procedure is like that adopted by Reyhner & Flügge-Lotz (1968), setting $u\,\partial/\partial x = 0$ in regions of reversed flow, justified in their problem by the fact that u is small in such regions. In contrast, for vortex flows u is not small and the justification for use of this condition (at the innermost radial station only) is instead that $\partial/\partial\xi = 0$ when the proper similarity variable is used. As will be seen in § 6, the conventional similarity variable $\eta = z/r^{\frac{1}{2}(1+n)}$ is proper only for $n < n_0 \doteq 0{\cdot}1217$; for $n_0 < n < 1$, the proper similarity variable for regions in which $f > 0$ is inferred in § 7.

Equations (4.3) were solved numerically using both explicit and implicit finite-difference schemes. Differences were centred in τ and ζ and uncentred in the downwind direction in ξ. Since the most extensive results were obtained using the implicit scheme, the explicit-difference equations will not be described here.

The finite-difference mesh was defined by the node-points

$$\xi_i = (i-1)\Delta\xi \quad (i = 1, 2, 3, \ldots, M+1),$$
$$\zeta_j = (j-1)\Delta\zeta \quad (j = 1, 2, 3, \ldots, N+1),$$

where $M = \xi_E/\Delta\xi$ and $N = \zeta_\infty/\Delta\zeta$. If q_{ij} represents a velocity component at time τ and q'_{ij} that at time $\tau + \Delta\tau$, the difference equations are written at the intermediate time $(\tau + \frac{1}{2}\Delta\tau)$ in the manner of Crank & Nicholson (1947). Thus, velocity components are replaced by mean values

$$q \to \bar{q}_{ij} = \tfrac{1}{2}(q'_{ij} + q_{ij}),$$

time derivatives by the centred difference

$$\partial q/\partial\tau \to (q'_{ij} - q_{ij})/\Delta\tau,$$

ζ derivatives by centred differences

$$\partial q/\partial\zeta \to (\bar{q}_{i,j+1} - \bar{q}_{i,j-1})/2\Delta\zeta,$$
$$\partial^2 q/\partial\zeta^2 \to (\bar{q}_{i,j+1} - 2\bar{q}_{i,j} + \bar{q}_{i,j-1})/(\Delta\zeta)^2,$$

and ξ derivatives by the uncentred differences

$$\partial q/\partial\xi \to (q_{i+1,j} - q_{ij})/\Delta\xi \quad \text{for} \quad f_{ij} > 0,$$
$$\partial q/\partial\xi \to (q_{ij} - q_{i-1,j})/\Delta\xi \quad \text{for} \quad f_{ij} < 0.$$

The ξ derivatives were evaluated at the old time τ, thus making the scheme

partially explicit. This was done to reduce computer storage requirements, since each ξ station is then uncoupled from the others, permitting iteration to completion at a given time step and ξ station without sweeping the entire mesh at each iteration. For a given time step, the equations were solved much as in the previous study of the potential vortex (Burggraf *et al.* 1971), using Gaussian elimination for simultaneous solution at all points at given ξ_i, τ, and iterating at each time step until a desired degree of convergence was obtained (say $|q' - q| < 10^{-5}$).

The numerical results exhibited two time scales; the radially inward flow next to the wall adjusted quickly, requiring a small time step for stability of the computation. However, the bulk of the flow appeared to possess a wave-like nature with much longer time required to settle down to a steady state. This problem is aggravated by increasing ξ_E; as a result, even though a variable time step was used, several thousand time steps were required to reach the steady state. A typical time step was $\Delta\tau = 0{\cdot}001$, at $\tau = 0$, although larger values were used as the computation progressed. All the results presented here were obtained with mesh size $\Delta\xi = 0{\cdot}1$ and $\Delta\zeta = 0{\cdot}3$, chosen as a compromise between accuracy and the practical requirements of storage capacity and computation time. The computations were performed by an IBM 360/75 digital computer. A typical computation time to advance 100 time steps for a flow region

$$0 \leqslant \xi \leqslant 3, \quad 0 \leqslant \zeta \leqslant 39{\cdot}9$$

was 2 minutes for the explicit program with short time step, and 6 minutes for the implicit program with longer time step.

The accuracy of the computations was assessed in two ways, first by comparison with available numerical solutions from earlier studies for the cases $n = -1, 0$ and $+1$, and second by checking the momentum-integral balance. For the radial balance, the momentum-integral equation is

$$\left[\frac{\partial f}{\partial \zeta}\right]_{\zeta=0} = -\left[\tfrac{3}{2}(1-n) - \frac{11-6n}{4}\exp(-\xi)\right]\int_0^\infty f^2 d\zeta + (1-\exp(-\xi))\frac{\partial}{\partial \xi}\int_0^\infty f^2 d\zeta + \int_0^\infty (g^2-1)\,d\zeta, \qquad (4.4)$$

and a similar expression holds for $[\partial g/\partial \zeta]_{\zeta=0}$. Thus the shear at the surface of the disk can be evaluated by integrating functions of the computed velocity profiles and compared with the shear evaluated by direct differencing of the same profiles. Generally the comparison was good as long as the mesh was sufficiently thick. A more explicit comparison will be given following the discussion of the velocity profiles.

Radial velocity profiles for $n = -1$(rigid rotation) are shown in figure 1. These profiles, corresponding to $\tau = 35{\cdot}0$, were computed for a region $0 \leqslant \xi \leqslant 2$, $0 \leqslant \zeta \leqslant 30$ using the explicit program with time step $\Delta\tau = 0{\cdot}01$. At $\tau = 35{\cdot}0$, the maximum time derivative in the flow field had been reduced to 0·048, compared with an initial value of 26·1. The residual unsteady motion appeared to be oscillatory with sufficiently small amplitude that the results in figure 1 are essentially those of steady flow. Boundary condition (1.2) with $\tilde{\beta} = 0$ was applied at the innermost radius $\xi = 2$, corresponding to a similarity requirement on the reversed

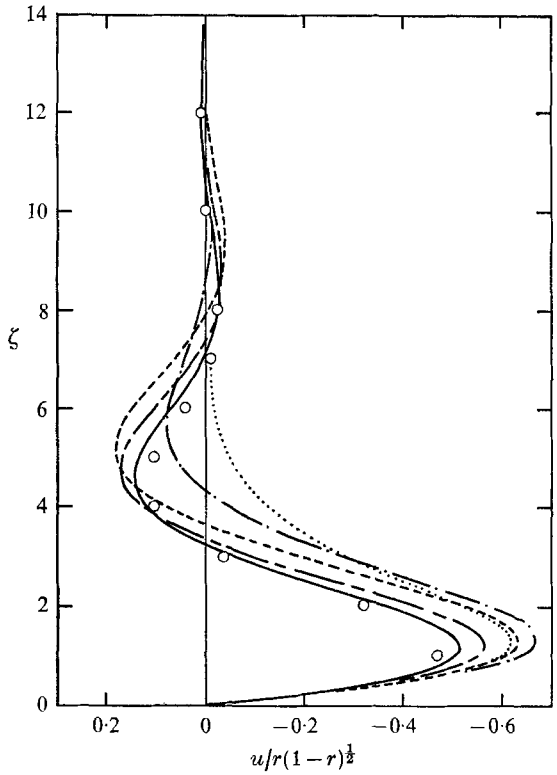

FIGURE 1. Radial velocity profiles, $n = -1$. r: ...., 1·0; — · —, 0·607; - - - -, 0·368; — · · —, 0·223; ——, 0·135; ○, Browning ($r = 0$).

flow. The encircled points in the figure are from the similarity solution of Browning (Schlichting 1968), corresponding to $r = 0$. King and Lewellen (1964) have obtained nearly identical results. As indicated by the results in figure 1, the peak value of the normalized radial velocity, $u/V(r)$, is a convex function of r, reaching its maximum at $r \approx 0{\cdot}4$. This behaviour seems to be quite reliable, since our computed values agree with $1\frac{1}{2}$ % with those of Anderson (1966), while the momentum-integral calculation of the radial surface shear checked with 2 % for $0 \leqslant \xi \leqslant 2$. The evidence for the Bödewadt similarity solution as the proper terminal solution for $r \to 0$ is actually stronger than indicated by figure 1; if the similarity solution is evaluated at the local radius, accounting for the factor $(1-r)^{-\frac{1}{2}}$, the computed results at $r = 0{\cdot}368$ deviate from the similarity solution by at most 2 % and those at $r = 0{\cdot}135$ by at most 1 %. It is also of interest that, in terms of the variables used here, the radial surface shear varies by at most 16 % over the entire disk (see table 1). The tangential surface shear, however, nearly doubles from the edge to the centre of the disk.

Similar results for the case $n = 0$ are shown in figure 2. The region in space was again $0 \leqslant \xi \leqslant 2$, $0 \leqslant \zeta \leqslant 30$. The explicit program was used with $\Delta\tau = 0{\cdot}001$ for $0 \leqslant \tau \leqslant 0{\cdot}5$ and $\Delta\tau = 0{\cdot}005$ for $0{\cdot}5 < \tau \leqslant 15{\cdot}5$. The maximum value of the time derivative was 0·006 at $\tau = 15{\cdot}5$, occurring at $\xi = 0{\cdot}6$ in the slow-to-settle outer region. The computation was continued to larger values of time with the

		$-f_\xi$				g_ξ			
ξ	r	$n=-1{\cdot}0$	$n=0{\cdot}0$	$n=0{\cdot}5$	$n=1{\cdot}0$	$n=-1{\cdot}0$	$n=0{\cdot}0$	$n=0{\cdot}5$	$n=1{\cdot}0$
0·0	1·000	1·0738*	1·0738*	1·0738*	1·0738*	0·4200*	0·4200*	0·4200*	0·4200*
0·5	0·607	1·1053	1·1059	1·0973	1·0885	0·5608	0·4459	0·3936	0·3423
1·0	0·368	1·0786	1·1299	1·1177	1·0938	0·6746	0·4528	0·3498	0·2613
1·5	0·223	1·0161	1·1466	1·1323	1·0920	0·7388	0·4583	0·3087	0·1963
2·0	0·135	0·9702	1·1533	1·1433	1·0881	0·7574	0·4617	0·2707	0·1453
2·5	0·082	—	—	1·1520	—	—	—	0·2362	—
3·0	0·050	—	—	1·1590	—	—	—	0·2053	—
∞	0	0·942†	1·201†	1·199‡	1·0866§	0·773†	0·443†	0·0‡	0·0§

TABLE 1. Normalized surface shear for steady flow. Mesh size: $\Delta\xi = 0{\cdot}1$, $\Delta\zeta = 0{\cdot}3$ (excepting referenced data).
* Mack (1962); † King & Lewellen (1964); ‡ §6; § Burggraf *et al.* (1971)

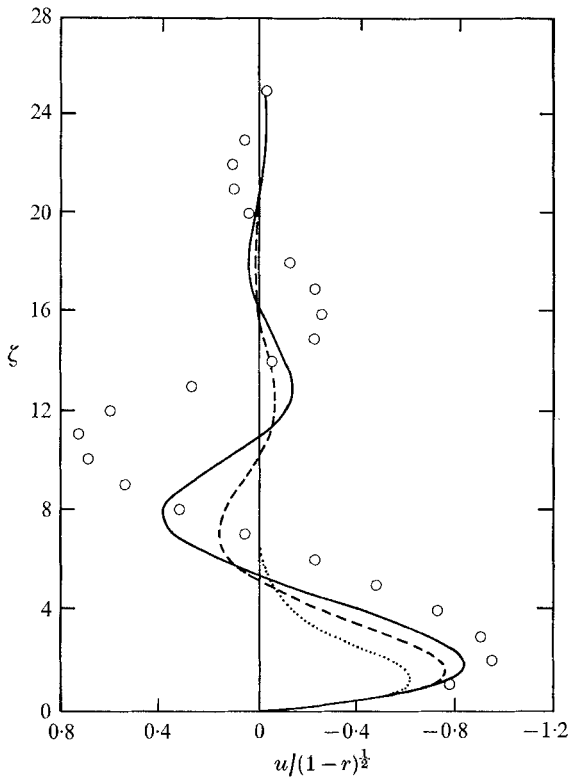

FIGURE 2. Radial velocity profiles, $n = 0$. Curves labelled as in figure 1. ○, King & Lewellen ($r = 0$).

implicit program with negligible changes in the results. The velocity profile near the wall, up to the first maximum, appears to be as close to the terminal similarity profile as it was for the case $n = -1$. Further from the wall, however, it is evident that similarity is approached much more slowly than for the case $n = -1$. The radial surface shear for $n = 0$ increases monotonically as r decreases, varying by about $12\frac{1}{2}$ % over the disk (table 1). In strong contrast to the case $n = -1$, the tangential surface shear for $n = 0$ is nearly constant, increasing by only 10 % from the edge to the centre of the disk. The momentum-integral values for the surface shear were within 4 % of the direct-difference values for $0 \leqslant \xi \leqslant 1{\cdot}9$.

The potential vortex, $n = 1$, was chosen as the third test case; the resulting steady-state radial velocity profiles are given in figure 3. The flow region included for the unsteady computation was again $0 \leqslant \xi \leqslant 2$, $0 \leqslant \zeta \leqslant 30$. The initial time step using the explicit program was 0·0001, but $\Delta\tau$ was increased to 0·0005 for $\tau > 0{\cdot}1$. The solution achieved its steady state, shown in figure 3, by the time $\tau = 1{\cdot}35$. Although the time step was drastically reduced in going from $n = -1$ to $n = +1$, the total number of time steps to achieve the steady state was approximately the same for each case. Noting that the variable τ is measured in units of radians of external flow rotation at the outer edge of the disk, and that the potential vortex rotates faster at smaller radii, it is reasonable that the boundary layer for the potential vortex should settle down to its steady state

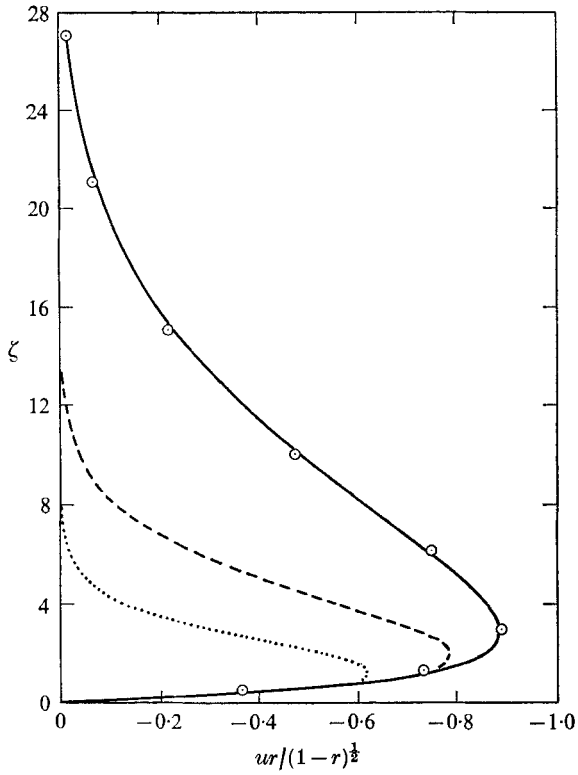

FIGURE 3. Radial velocity profiles, $n = 1$. Curves labelled as in figure 1. ⊙, Burggraf *et al.* ($r = 0{\cdot}135$).

much faster than that for rigid rotation. The encircled points are samples from the more accurate computation obtained by direct solution of the steady-flow equations (Burggraf *et al.* 1971). We attribute the difference between those results and the present results to the coarser mesh used in the unsteady program. Note that no boundary condition at $r_E = 0{\cdot}135$ was utilized for this case, since the radial flow is everywhere toward the axis.

From the evidence of the three test cases discussed above, we see that when similarity exists, it serves as a terminal solution for the flow near the axis, that the boundary condition (1.2) applied at the inner radius of the mesh produces the expected similarity behaviour, and that the finite-difference method and mesh characteristics used here provide results sufficiently accurate to reveal the structure of the various types of vortex boundary layers. With this assurance, we now turn to the case $n = \frac{1}{2}$, for which no earlier solutions are available.

5. Numerical results for $n = 0{\cdot}5$

We have proposed in Burggraf, Stewartson & Belcher (1971) that a simple similarity solution is not the proper terminator of the boundary layer for $r \to 0$ if $n > 0{\cdot}1217$, and in fact a double-structured boundary layer was shown to be consistent with numerical results for $n = 1$. However, for $n = 1$, the boundary

layer does not exhibit reversed flow, as would be expected for $n < 1$. To test our multiple-structure hypothesis for $n < 1$, it was decided to numerically compute the boundary layer for the generalized vortex with $n = \frac{1}{2}$, medial in the expected range of non-similarity $0{\cdot}1217 < n < 1$.

Initially the explicit program was used for the region $0 \leqslant \xi \leqslant 2$, $0 \leqslant \zeta \leqslant 39{\cdot}9$, with $\Delta\tau = 10^{-4}$ for $0 \leqslant \tau \leqslant 0{\cdot}05$ and $\Delta\tau = 0{\cdot}001$ for $0{\cdot}05 \leqslant \tau \leqslant 2{\cdot}55$. When $\tau = 2{\cdot}55$, the profiles were approximately stationary, but it appeared that a closer approach to the axis would be necessary. Extending the region to $\xi_E = 3$ with the explicit program, the initial time step had to be reduced to 10^{-5}, requiring excessive computer time. The implicit program was then developed, permitting stable computations for $\xi_E = 3$ with a time step of 10^{-2}. Nearly stationary profiles were then attained over the extended region at $\tau = 2{\cdot}83$. In making these calculations, condition (1.2) with $\tilde{\beta} = \frac{3}{4}$ had been applied at boundary points $\xi = \xi_E$ for which $f > 0$. One effect of extending the mesh from $\xi_E = 2$ to $\xi_E = 3$ was to produce changes of 20 % in the maximum value of the steady reversed-flow speed at $\xi = 2$. Furthermore, condition (1.2) was not satisfied even approximately at points on the boundary $\xi_E = 3$ for which $f < 0$. Consequently, either $\xi_E = 3$ ($r_E = 0{\cdot}050$) is not small enough or $\tilde{\beta}$ in (1.1) should not be the similarity value of $\frac{3}{4}$. When simple similarity fails a generalization of the earlier analysis of the potential vortex (cf. §7) suggests that the appropriate outer variable is that of (1.1) with $\tilde{\beta} = 0{\cdot}281$ for $n = \frac{1}{2}$. Using this value in condition (1.2), the computations were continued to $\tau = 2{\cdot}87$, by which time the solution had again achieved nearly steady-state conditions. The ξ derivatives at $\xi_E = 3$ for $f < 0$ were now small and, as will be seen, these numerical results are consistent with the analytical structure given in §6 and §7.

The computed flow pattern in the boundary layer for $n = \frac{1}{2}$ is shown in figure 4, in terms of the (ξ, ζ) co-ordinate system. Over the outer half of the disk

$$(0 < \xi < 0{\cdot}7)$$

the flow is everywhere downward toward the surface, while the flow is primarily upward over the inner half of the disk. The oscillations in the radial flow build up quite rapidly as ξ increases, with apparently ever-increasing amplitude. The peaks and troughs of the streamline contours appear to exhibit similarity behaviour along the upward curving contours labelled† $Z = 3{\cdot}282$ and $Z = 6{\cdot}565$, where $Z = z/r^{0{\cdot}281}$, consistent with the boundary condition applied at ξ_E. For later reference, the inviscid nature of the flow in this region is suggested by the nearly constant value of rv ($\approx 0{\cdot}37$) indicated by the numerical values at tagged points on the streamline $\psi = -0{\cdot}30$.

The radial development of the steady velocity profiles is shown in figures 5–7. In each of these figures two solutions are presented, the dashed curves for boundary condition (1.2) with $\tilde{\beta} = 0{\cdot}750$, and the solid curves for (1.2) with $\tilde{\beta} = 0{\cdot}281$.

Near the surface the radial flow, figure 5, exhibits a self-similar behaviour in that the three profiles shown for $r = 0{\cdot}368$, $0{\cdot}135$, and $0{\cdot}050$ approach a single

† The significance of the numerical values 3·282 and 6·565 is explained in §7.

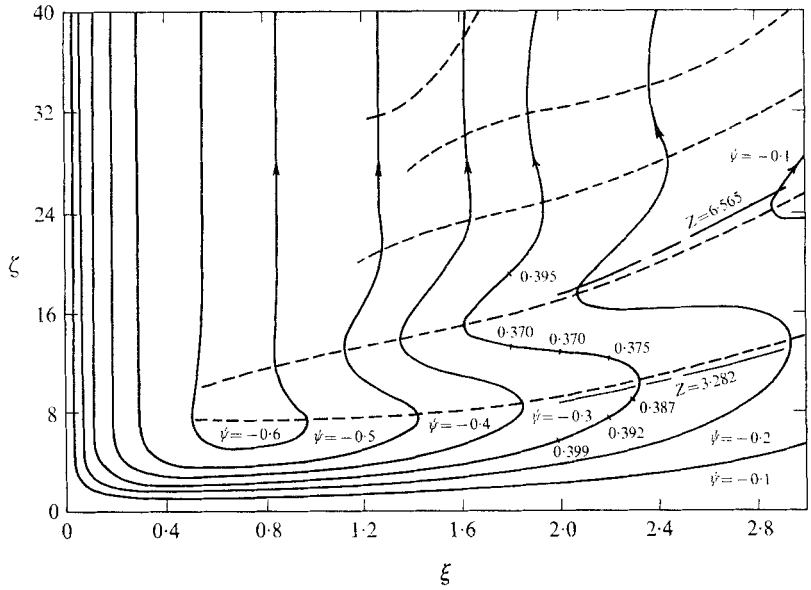

FIGURE 4. Streamline contours, $n = 0{\cdot}5$. ——, streamlines; - - - - -, $u = 0$. Numbers along streamline $\psi = -0{\cdot}3$ indicate value of rv at tagged point.

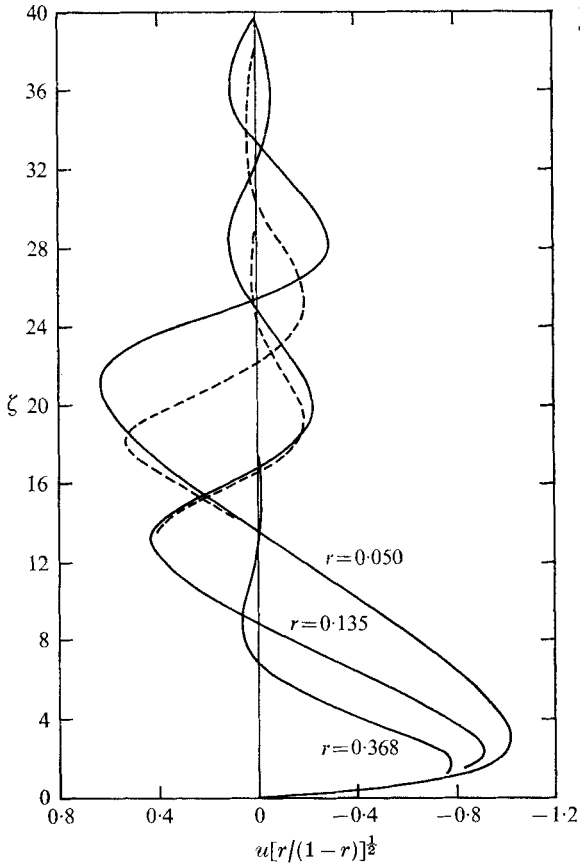

FIGURE 5. Radial velocity profiles, $n = 0{\cdot}5$. ——, boundary condition (1·1) with $\tilde{\beta} = 0{\cdot}281$; - - - - -, boundary condition (1·1) with $\tilde{\beta} = 0{\cdot}750$.

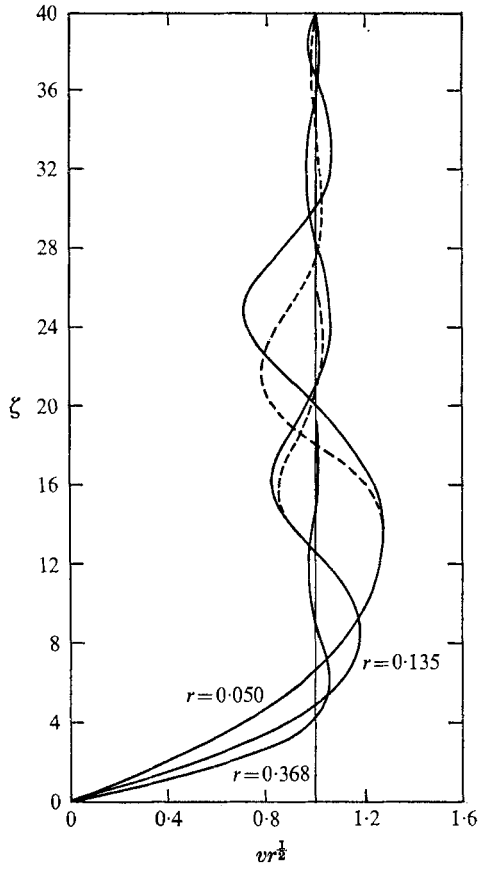

FIGURE 6. Azimuthal velocity profiles, $n = 0{\cdot}5$. Curves labelled as in figure 5.

asymptote near $\zeta = 0$. By contrast, the outer flow exhibits no such behaviour, and the profiles appear to be diverging rapidly as $r \to 0$. This behaviour is quite unlike that shown for the cases $n = -1$ and $n = 0$, which suggested self-similarity for all ζ when $r \to 0$, but instead is much like the double-layered structure of the boundary layer for the potential vortex (Burggraf *et al.* 1971). On the other hand, the tangential velocity profiles of figure 6 appear to diverge for all $\zeta > 0$, which again reminds us of the potential vortex, for which the tangential velocity in the lower deck of the boundary layer vanishes relative to the radial velocity in the limit $r \to 0$. Consequently these numerical results for $n = \frac{1}{2}$ confirm the idea of a multi-structured terminal boundary layer. It is significant in figure 5 that the thickness of the region, for which $\partial f/\partial\zeta$ is positive, grows rapidly as r decreases, whereas the region immediately above, for which $\partial f/\partial\zeta$ is negative, has about the same thickness for each value of r.

The vertical velocity, shown in figure 7, at first sight gives the appearance of erratic behaviour. The trends shown are supported by the analysis, however. Near the surface, a small region of downflow appears, not appearing in the results for $n = -1$ or $n = 0$. For similarity solutions we introduce a stream function as

$$r^n u = \Psi_0'(\eta), \quad \eta = zr^{-\frac{1}{2}(n+1)}.$$

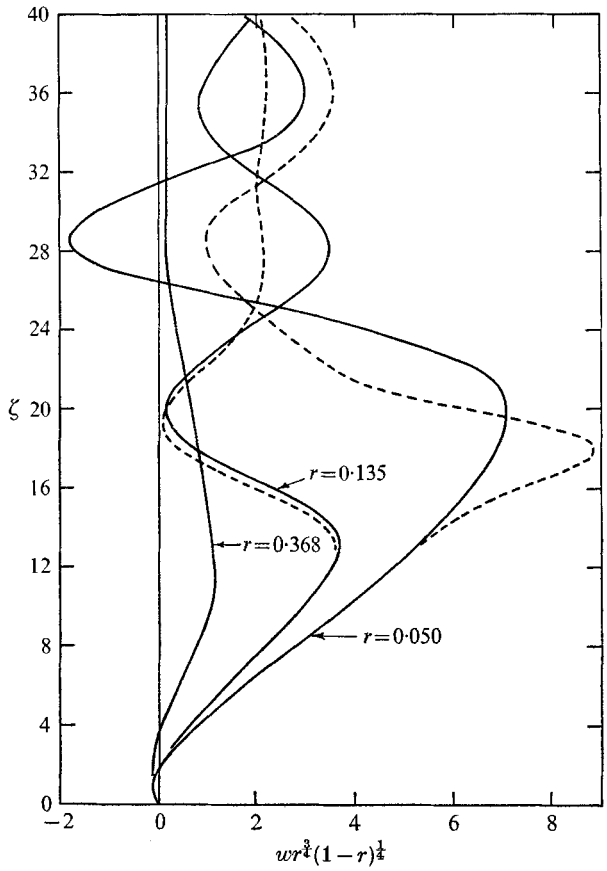

FIGURE 7. Vertical velocity profiles, $n = 0{\cdot}5$. Curves labelled as in figure 5.

Then continuity of mass requires that the vertical velocity should satisfy

$$wr^{\frac{1}{2}(n+1)} = \tfrac{1}{2}(n-3)\Psi_0(\eta) + \tfrac{1}{2}(n+1)\eta\Psi_0'(\eta).$$

Sufficiently near the wall, $r^n u \propto -\eta$, so that

$$wr^{\frac{1}{2}(n+1)} \propto -\tfrac{1}{4}(3n-1)\eta^2.$$

Hence a downflow region develops near the surface for $n > \frac{1}{3}$, gradually increasing in extent with increasing n, until it covers the entire boundary layer for $n = 1$. Above this downflow region (for $n = \frac{1}{2}$), w increases nearly linearly with ζ until u changes sign at about $\zeta = 13{\cdot}5$. The slope and the peak value of w in this linear region increase as $r \to 0$, consistent with the asymptotic behaviour of the inner viscous region analysed in §6. Above $\zeta \approx 13{\cdot}5$, the radial velocity changes sign, and boundary condition (1.2) comes into play. Following the solid curves in figure 7, for $\tilde{\beta} = 0{\cdot}281$, the upflow quickly peaks at about the same point as the negative peak in u, and a second and larger downflow region develops for $r = 0{\cdot}050$. This again is consistent with the analysis of §7, which indicates that u returns from its peak positive value to a new peak negative value through a thin viscous

shear layer, and that in this layer w is proportional to u for sufficiently small r. The behaviour of the graph in figure 7 strongly supports this analytical description in the range $20 < \zeta < 28$.

It is evident in figures 5–7 that a thicker mesh would be desirable, since the slopes of the velocity profiles are not negligible at $\zeta_\infty = 39{\cdot}9$. This problem is especially visible in the momentum-integral check, which, as the radius is reduced, serves as a progressively deteriorating standard for the surface shear. Over the range $0{\cdot}135 \leqslant r \leqslant 1$, the momentum-integral values for the surface shear differed by up to 8 % from the direct-difference values. The effect of insufficient mesh thickness was especially pronounced at smaller radii, with the momentum-integral value of radial shear plunging to 20 % of the direct-difference value at $r = 0{\cdot}050$. This difficulty was observed previously in the computation for the potential vortex (Burggraf *et al.* 1971), where the problem was cured by increasing mesh thickness with little change thereby produced in the velocity profiles, except near the outer edge of the mesh. Similarly, we feel that the present calculations for the generalized vortex with $n = \frac{1}{2}$ are quite satisfactory except near the outer edge of the mesh, and it is shown in table 1 that the values of wall shear obtained by direct-differencing agree very well with the theoretical structure developed in §6.

6. Terminal behaviour: the wall layer

The main conclusion we draw from the numerical studies is that a single-structured self-similar velocity profile is very unlikely to exist in the limit $r \to 0$ when $n = \frac{1}{2}$. In the theoretical study described §6 and §7, we shall make the assumption that no such structure exists, and look instead for analogous results to those found when $n = 1$. For that vortex it was shown by Burggraf *et al.* that, instead of a single terminal structure, the velocity profile must be divided into two parts: an inner layer in which viscous forces are significant and the motion of the fluid is largely directed radially inwards towards the axis, and an outer layer in which viscous forces may be neglected. Our aim in §6 is to give a corresponding study for a swirling flow with $n = \frac{1}{2}$, and also to discuss other values of n for which the ideas might be relevant.

We make the same assumptions as for $n = 1$, namely that the motion is self-similar, and viscous forces are important but that $u^2 \gg v^2$. Then the similarity variable must be $\eta = z/r^{\frac{1}{2}(1+n)}$ and, on writing

$$\psi = r^{\frac{1}{2}(3-n)}\Psi_0(\eta), \tag{6.1}$$

we find that

$$\Psi_0''' + \tfrac{1}{2}(3-n)\Psi_0\Psi_0'' + n\Psi_0'^2 = 1, \tag{6.2a}$$

with boundary conditions

$$\Psi_0(0) = \Psi_0'(0) = 0, \quad \Psi_0'(\infty) = -n^{-\frac{1}{2}}. \tag{6.2b}$$

The condition on Ψ_0' as $\eta \to \infty$ is partly fixed by the requirement that viscous forces become negligible when $\eta \gg 1$ and so $n\Psi_0'^2 \to 1$. The sign of $\Psi_0'(\infty)$ can be

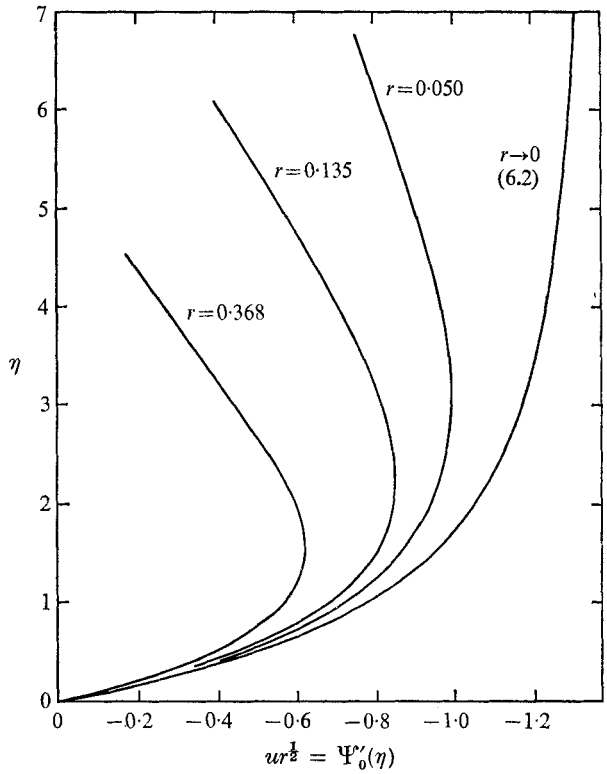

FIGURE 8. Approach to terminal structure; radial velocity profiles in the wall layer, $n = 0{\cdot}5$.

decided from the physical argument that, in the absence of an azimuthal velocity, the effective pressure gradient V^2/r must drive the fluid radially inwards, towards the axis. The numerical studies confirm the choice of sign. The governing equation is one of the family of Falkner–Skan equations, and is an example of the backward-facing boundary layer studied by Goldstein (1965). It may easily be shown that, when $\eta \gg 1$,

$$r^n u \sim \Psi_0' = -\frac{1}{\sqrt{n}} + C^{(0)}\eta^{-4n/(3-n)} + \ldots, \tag{6.3}$$

where $C^{(0)}$ is a constant and for $n = \frac{1}{2}$ has been computed to be 0·384. In figure 8 a comparison is made between the solution of (6.2) and the numerical solution of the finite disk problem at various values of r.

It seems certain that real solutions of (6.2) exist for all $n > 0$, but there clearly are no real solutions if $n < 0$, so that we may conclude that a multiple structure of the kind we have in mind here is impossible if $n < 0$. This is in line with our numerical results when $n = -1$, and with the successful computation of the equations governing a simple terminal structure when $n < 0$. We shall now demonstrate that the structural properties of v in the lower layer provide an even more stringent condition on n for the existence of a multiple terminal structure.

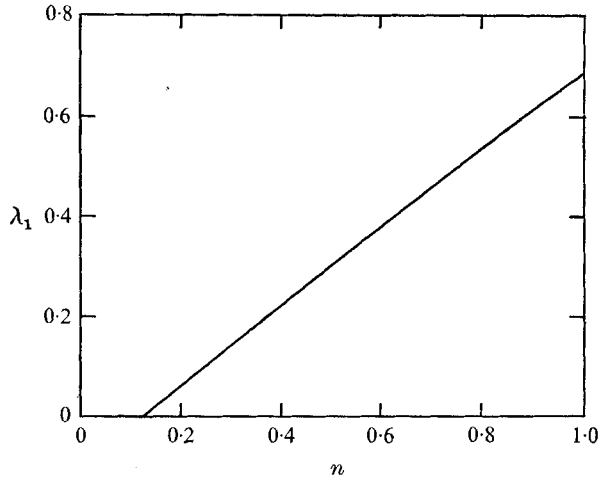

FIGURE 9. Fundamental eigenvalues for the azimuthal flow.

For, as we have already seen in the discussion of the solution when $n = 1$, if ψ is given by (6.1) and (6.2) the appropriate form for v when $r \ll 1$ is of the form

$$r^n v = r^\lambda \gamma_\lambda(\eta), \tag{6.4}$$

where λ must be chosen so that the viscous term in the equation governing γ_λ is negligible when $\eta \gg 1$. On substituting into the azimuthal equation (2.5), we find that γ_λ satisfies

$$\gamma_\lambda'' + \tfrac{1}{2}(3-n)\Psi_0\gamma_\lambda' - (\lambda+1-n)\Psi_0'\gamma_\lambda = 0, \tag{6.5}$$

subject to $\gamma_\lambda(0) = 0$. Since $\psi_0' \to -n^{-\frac{1}{2}}$ as $\eta \to \infty$, it follows that for general λ, $|\gamma_\lambda|$ increases exponentially with η; only for a discrete set λ_i ($i = 1, 2, 3, \ldots$) of values of λ can $|\gamma_\lambda|$ grow algebraically with η, in order that the viscous term in (6.5) is negligible when $\eta \gg 1$. Thus, if $n = \frac{1}{2}$, the first few values of λ_i are

$$\lambda_1 = 0{\cdot}3003, \quad \lambda_2 = 2{\cdot}5178, \quad \lambda_3 = 4{\cdot}7819, \quad \lambda_4 = 7{\cdot}0727.$$

An essential requirement for the success of the line of argument being pursued in this section, however, is that $\lambda_i > 0$, for otherwise the basic assumption $u^2 \gg v^2$ is violated. A numerical study of the smallest value of λ for various n, summarized in figure 9, leads to the conclusion that $\lambda_i > 0$ for all i only if $n > 0{\cdot}1217$. Hence, our assumption of a multiple structure breaks down if

$$n < 0{\cdot}1217,$$

which is a stronger criterion than that ($n < 0$) deduced from the equation for ψ_0.

In the particular case $n = \frac{1}{2}$, a check on the validity of the model can be made by comparing the computed value of $\partial v/\partial z$ (using the data of table 1) with the form predicted by (6.4), using the lowest acceptable value of λ, namely 0·3003. It is found that

$$r^{(3n-\lambda)/2}\partial v/\partial z \tag{6.6}$$

is very nearly constant and seems to be approaching 0·512 as $r \to 0$. Using this number to provide a numerical factor for $\gamma_{\lambda_1}(\eta)$, a comparison was made between

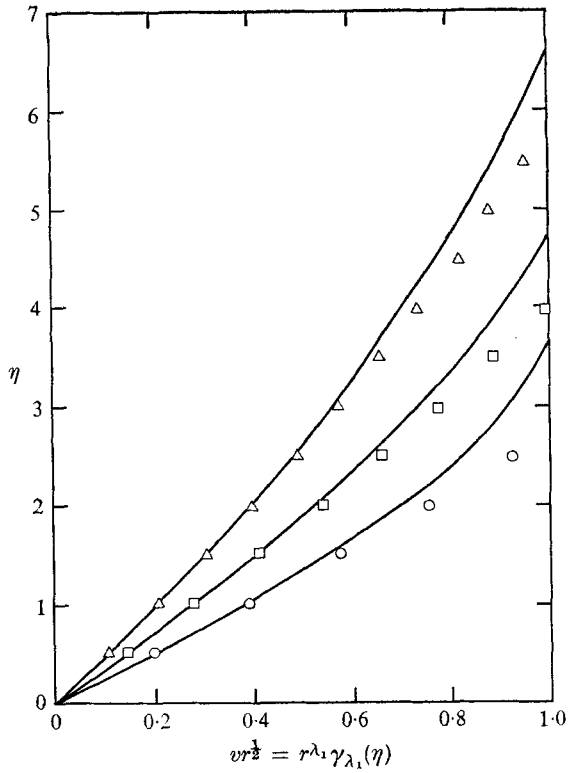

FIGURE 10. Comparison of azimuthal velocity profiles with asymptotic formula for wall layer, $n = 0{\cdot}5$. ——, (6.4); plotted points, numerical solution. r: ○, 0·368; □, 0·135; △, 0·050.

the computed profiles and the fundamental similarity profile; it is displayed in figure 10. The agreement shown there, and in figure 8, is sufficiently encouraging for us to claim, with confidence, that (6.1) and (6.4) correctly describe the structure of the inner layer as $r \to 0$.

Let us now consider the behaviour of (u, v) as $\eta \to \infty$ and the inner layer merges with the outer structure. From (6.5), since γ_λ is algebraic at infinity and

$$n^{\frac{1}{2}}\psi_0' \approx -1,$$

$$\gamma_{\lambda_i} \approx A_i[\eta n^{-\frac{1}{2}}]^{2(\lambda_i+1-n)/(3-n)} \quad \text{as} \quad \eta \to \infty, \tag{6.7}$$

or

$$r^{1+\lambda_i-n}\gamma_{\lambda_i} \approx A_i[-\psi]^{2(\lambda_i+1-n)/(3-n)} \quad \text{as} \quad \eta \to \infty. \tag{6.8}$$

The A_i are constants to be found; in particular, by fitting the solution of (6.5) to the numerical results given in figure 6, we find $A_1 = 0{\cdot}790$.

In addition to the eigenvalues associated with (6.5), the equation for Ψ_0' has eigenvalues that also make a contribution to the form of v when $\eta \gg 1$. However, this contribution appears through forcing terms on the right-hand side of (6.5) arising only from the inviscid terms in (2.5). It follows that the contribution is absorbed into ψ when the form (6.8) is used, and we conclude that, when $\eta \gg 1$,

$$rv \approx \sum_{i=1}^{\infty} r^{1+\lambda_i-n}\gamma_{\lambda_i} \approx \sum_{i=1}^{\infty} A_i(-\psi)^{2(\lambda_i+1-n)/(3-n)}. \tag{6.9}$$

The eigenvalues associated with (6.2) can be found by writing

$$\psi = r^{\frac{1}{2}(3-n)}[\Psi_0(\eta) + r^{\mu}\Psi_{\mu}(\eta) + \ldots], \tag{6.10}$$

substituting in (2.4) and neglecting v^2 and Ψ_{μ}^2. A linear ordinary differential equation of a type similar to (5.5) then results for Ψ_{μ}. On requiring that the viscous term Ψ_{μ}''' is negligible when $\eta \gg 1$ or, equivalently, that the growth rate of Ψ_{μ} is then algebraic, we find that μ must take on a discrete set of values $\mu_i (i = 1, 2, 3, \ldots)$, of which the four lowest are

$$\mu_1 = 2{\cdot}4679, \quad \mu_2 = 4{\cdot}6745, \quad \mu_3 = 6{\cdot}9269, \quad \mu_4 = 9{\cdot}2072, \tag{6.11}$$

when $n = \frac{1}{2}$. On examining the form of Ψ_{μ} when $\eta \gg 1$, it may be verified that

$$\Psi_{\mu} \approx Br^n(-\Psi_0 r^{(3-n)/2})^{2(\mu-2n)/(3-n)}. \tag{6.12}$$

The discussion of the conversion of the structure revealed by (6.12) into a form of u appropriate to the structure of the outer layer analogous to (6.9) will be dealt with in § 7.

7. Terminal behaviour: the ladder structure

On leaving the inner layer ($\eta \gg 1$), the viscous terms in the governing equations are negligible. This requirement from the theoretical analysis of § 6 is borne out by the trends of the numerical results, so we shall assume that above the wall layer a region exists in which the viscous terms remain small compared with the inertia terms. In that event, two integrals of the governing equations can be written down. The best way of obtaining them is to use von Mises co-ordinates (r, ψ), when, without any approximation, the governing equations may be written as

$$u\frac{\partial u}{\partial r}\bigg|_{\psi} = \frac{v^2}{r} - \frac{1}{r^{1+2n}} + ru\frac{\partial}{\partial \psi}\left(ru\frac{\partial u}{\partial \psi}\right), \tag{7.1}$$

and

$$u\frac{\partial (rv)}{\partial r}\bigg|_{\psi} = ru\frac{\partial}{\partial \psi}\left(ru\frac{\partial}{\partial \psi}(rv)\right). \tag{7.2}$$

If viscous terms are negligible, then the right-hand side of (7.2) may be neglected, and it may then be integrated to yield

$$rv = G(\psi), \tag{7.3}$$

G being an arbitrary function. The physical interpretation of (7.3) is that the angular momentum is conserved on a streamline. The form of G when ψ is small must match with (6.9), the asymptotic expansion of rv when η is large.

On multiplying (7.1) by $2u$, (7.2) by $2v/r$ and adding, we obtain

$$u\frac{\partial}{\partial r}\left(u^2 + v^2 - \frac{1}{nr^{2n}}\right) = 2r^2u^2\frac{\partial}{\partial \psi}\left(u\frac{\partial u}{\partial \psi}\right) + 2r^2uv\frac{\partial}{\partial \psi}\left(u\frac{\partial v}{\partial \psi}\right). \tag{7.4}$$

If viscous forces are negligible for the radial flow also, then

$$u^2 + v^2 - \frac{1}{nr^{2n}} = F(\psi), \tag{7.5}$$

where F is an arbitrary function of ψ. The physical interpretation of this result is that it is a version of Bernoulli's equation, $n^{-1}r^{-2n}$ being the effective reduced pressure in the boundary layer. The form of F when ψ is small must match with the asymptotic expansion of the left-hand side of (7.5) in the inner layer when η is large. The contribution to the asymptotic expansion of u from the asymptotic expansion of v is taken care of by the term v^2 in (7.5), so that F is explicitly independent of (6.9). There will clearly be contributions from the eigenfunctions of ψ, (6.12), and from the asymptotic structure of ψ, (6.3). No interaction terms will be present, because the inviscid term in (7.1) is linear in u^2. We conclude that

$$F(\psi) \sim \sum_{i=0}^{\infty} C_i(-\psi)^{2(\mu_i-2n)/(3-n)}, \tag{7.6}$$

where μ_i, $i \geqslant 1$, are the eigenvalues (6.11); the C_i, $i \geqslant 1$, are constants to be found, $\mu_0 = 0$ and $C_0 = -1{\cdot}433$, if $n = \frac{1}{2}$, from (6.3).

If we knew F and G explicitly, another integral would follow on writing $u = r^{-1}\partial\psi/\partial z$, so that

$$\frac{1}{r^2}\left(\frac{\partial\psi}{\partial z}\right)^2 = \frac{1}{nr^{2n}} + F(\psi) - \frac{G^2(\psi)}{r^2}, \tag{7.7}$$

and a single integration would give ψ as a function of z and r. It follows from (7.7) that $|\psi| \ll 1$ when $r \ll 1$, so we can replace F and G by the leading terms of their asymptotic expansion, whence

$$\frac{1}{r^2}\left(\frac{\partial\psi}{\partial z}\right)^2 = \frac{1}{nr^{2n}} + C_0(-\psi)^{-4n/(3-n)} - \frac{1}{r^2}A_1^2(-\psi)^{4(\lambda_1+1-n)/(3-n)}. \tag{7.8}$$

In turn, (7.8) shows that $|\psi|$ cannot become too small, for $-\psi$ has a minimum value $O(r^{(3-n)/2})$. This condition is consistent with the known property of ψ on leaving the inner layer, namely that $(-\psi)r^{-(3-n)/2} = -\Psi' \gg 1$. In fact, we see that, as $r \to 0$, the term proportional to C_0 may be neglected, and then (7.8) leads to a similarity form for ψ, viz.

$$\psi = r^{1-n+\beta}H(Z), \tag{7.9a}$$

where $Z = z/r^\beta$, $\qquad \beta = \dfrac{1-n}{2}\left(\dfrac{1+n-2\lambda_1}{1-n+\lambda_1}\right)$,

and

$$H'^2 = \frac{1}{n} - A_1^2(-H)^{4(\lambda_1+1-n)/(3-n)}, \tag{7.9b}$$

with $H(0) = 0$. Hence Z is given in terms of H as the incomplete Beta function

$$B_t\left(\frac{3-n}{1-n+\lambda_1}, \frac{1}{2}\right), \quad t = nA_1^2(-H)^{4(\lambda_1+1-n)/(3-n)}.$$

Further, from (7.5), recognizing that $F(\psi) \to 0$ as $r \to 0$ with Z fixed, we find that

$$r^n v \sim \left\{\frac{1}{n} - [H'(Z)]^2\right\}^{\frac{1}{2}}. \tag{7.10}$$

Thus, as Z increases from zero, so does $u = r^{-n}H'(Z)$, until at $Z = Z_{\frac{1}{2}}$ ($= 3{\cdot}282$ for $n = \frac{1}{2}$) u becomes positive. We have now arrived at a new situation in which the

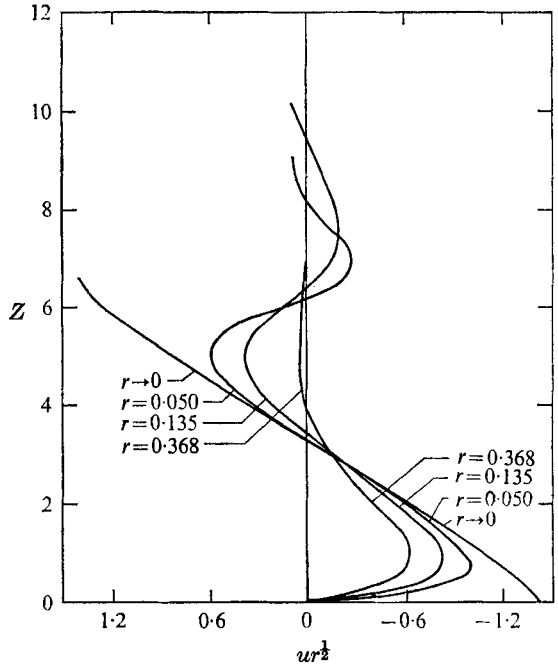

FIGURE 11. Approach to terminal structure: radial velocity profiles in outer region, $n = 0{\cdot}5$. Curve labelled $r \to 0$ corresponds to $H'(Z)$, (7.9*b*).

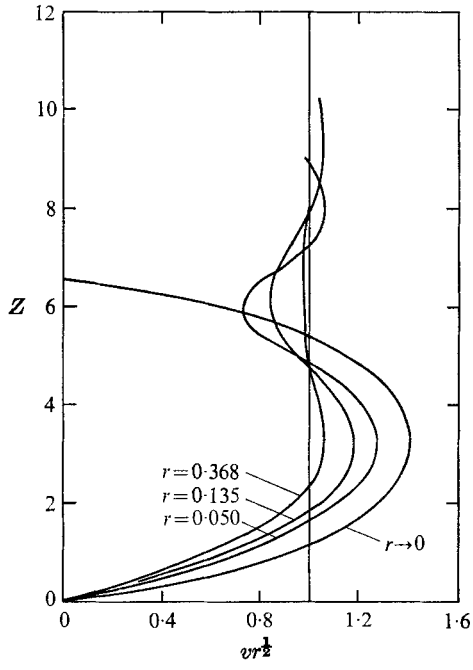

FIGURE 12. Approach to terminal structure: azimuthal velocity profiles in outer region, $n = 0{\cdot}5$. Curve labelled $r \to 0$ corresponds to (7.10).

velocity profile is no longer a terminal profile, but must be assigned at the terminating line $r = r_E$ of the numerical integration.

For $Z < Z_{\frac{1}{2}}$ conditions are not prescribed at r_E, since $u < 0$ there, so we can confidently expect a favourable comparison between this asymptotic theory and the numerical solution. This proves to be the case, as may be seen from figure 11, in which we draw the calculated values of $r^{\frac{1}{2}}u$ as functions of Z at various values of r (taking $n = \frac{1}{2}$ with $\beta = 0{\cdot}281$), and figure 12, in which we draw the calculated values of $r^{\frac{1}{2}}v$ and compare with $H'(Z)$. In both graphs the velocity profiles are clearly asymptoting to the expected limits.

When $u > 0$ (i.e. for a range of values of $Z > Z_{\frac{1}{2}}$), the form of the solution depends on the boundary conditions imposed on (u, v) at $r = r_E$. As explained in §5, various conditions were used in the computation, and the most consistent was that which assumed that the velocity profiles are self-similar with similarity parameter $Z = z/r^{\beta}$. The numerical solutions obtained with this condition were used in drawing figures 11 and 12. We see that the favourable comparison between the asymptotic theory and the numerical computation, already noticed when $Z < Z_{\frac{1}{2}}$, extends to the values of $Z > Z_{\frac{1}{2}}$ as well.

According to (7.8) or (7.9*b*), $r^n u$ increases from the value $-n^{-\frac{1}{2}}$ at $Z = 0$ until it reaches the value $+n^{-\frac{1}{2}}$ at $Z = Z_1$ ($= 6{\cdot}565$ for $n = \frac{1}{2}$), when $r^{-1+n-\beta}\psi = H$ is zero once more. Viscous forces must now become important, for otherwise there would have to be an unacceptable change in the sign of ψ, and we can expect a rapid transition in $r^n u$ back to the value $-n^{-\frac{1}{2}}$, through a shear layer similar in structure to (6.1), (6.2). The only difference is that the boundary conditions are changed to

$$\left.\begin{aligned} &\Psi' \sim n^{-\frac{1}{2}} = C^{(0)}(-\eta_1)^{4n/(3-n)} \quad \text{as} \quad \eta_1 \to -\infty, \\ \text{and} \quad &\Psi' \sim -n^{-\frac{1}{2}} + C^{(1)}\eta_1^{4n/(3-n)} \quad \text{as} \quad \eta_1 \to +\infty, \end{aligned}\right\} \tag{7.11}$$

where $\eta_1 = (z - Z_1 r^{\beta})/r^{(1+n)/2}$ is the new independent variable, $C^{(0)}$ is the constant defined in (6.3), and $C^{(1)}$ is to be found. A numerical integration taking $n = \frac{1}{2}$ shows that a solution to (6.2*a*) and (7.11) exists with the properties $\Psi(0) = -1{\cdot}125$ $\Psi''(0) = -0{\cdot}594$ where, without loss of generality, we have taken $\Psi'(0) = 0$ (see figure 13). The appropriate value of $C^{(0)}$ is $0{\cdot}384$ and the computed value of $C^{(1)}$ is $0{\cdot}745$, greater than $C^{(0)}$. A viscous transition also occurs in v, with a structure similar to that given by (6.4), (6.5). The only differences are that Ψ now satisfies (7.11), $\lambda = \lambda_1$, and the boundary conditions on γ_λ change to

$$\left.\begin{aligned} \gamma_\lambda &\sim A^{(0)}(-\Psi)^{2(\lambda_1+1-n)/(3-n)} \quad \text{as} \quad \eta_1 \to -\infty, \\ \gamma_\lambda &\sim A^{(1)}(-\Psi)^{2(\lambda_1+1-n)/(3-n)} \quad \text{as} \quad \eta_1 \to +\infty. \end{aligned}\right\} \tag{7.12}$$

Here $A^{(0)}$ is the constant A_1 defined in (6.8), and $A^{(1)}$ has to be found. For $n = \frac{1}{2}$, $A^{(0)} = 0{\cdot}790$, and $A^{(1)}$ is computed to be $1{\cdot}195$.

The vertical velocity in this transitional layer is given by

$$rw = -\frac{\partial \psi}{\partial r} = \beta r^{\beta-n} Z_1 \Psi'(\eta_1) + r^{(1-n)/2}\left[\frac{n-3}{2}\Psi(\eta_1) + \frac{n+1}{2}\eta_1 \Psi'(\eta_1)\right]. \tag{7.13}$$

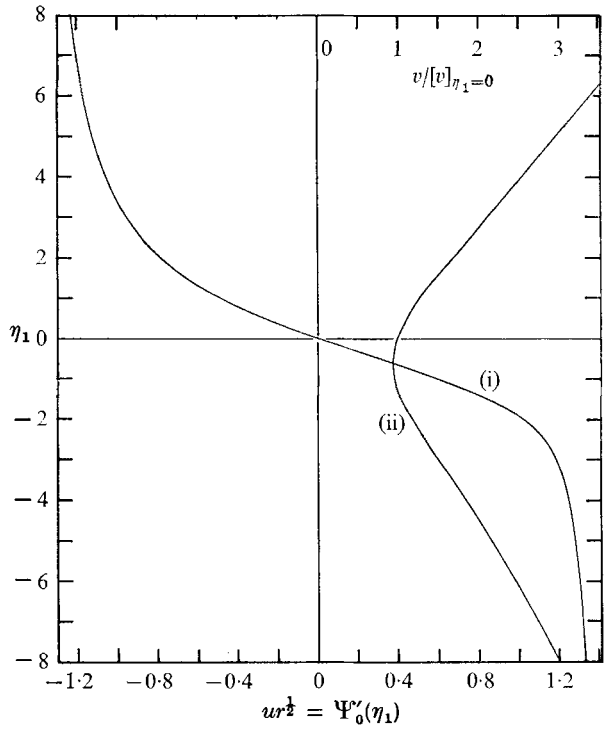

FIGURE 13. Terminal velocity profiles in the lowest free shear layer, $n = 0{\cdot}5$. Curve (i), lower scale; curve (ii), upper scale.

Since $r^n u = \Psi'(\eta_1)$, we see that, as $r \to 0$, $w/u \to \beta Z_1 r^{\beta-1}$, which is just the slope of the transitional layer. This property of w was noted at the end of § 5.

In figure 4 the significance of the curves on which $u = 0$ is now clear. These represent alternately the midpoints of the thick inviscid regions and those of the thin free viscous layers in the ladder structure. In particular, the point where $u = 0$ in the lowest inviscid region corresponds to $Z = 3{\cdot}282$. The lowest free viscous shear layer is centred at the discontinuity of the inviscid structure at $Z = 6{\cdot}565$, and for convenience is compared with the locus of points for which $u = 0$. The comparison is good at both levels, although slightly better at $Z = 3{\cdot}282$. It may be noted that, near $Z = 3{\cdot}282$, our use of boundary condition (1.2) with $\tilde{\beta} = 0{\cdot}281$ in the numerical calculation is correct, but near $Z = 6{\cdot}565$ two values of $\tilde{\beta}$ would be required by the asymptotic structure: $\tilde{\beta} = 0{\cdot}281$ in the inviscid region where $f > 0$, $\partial f/\partial\zeta > 0$, and $\tilde{\beta} = 0{\cdot}750$ in the viscous region where $f > 0$, $\partial f/\partial\zeta < 0$. This slight inconsistency appears to be of little consequence, since the displacement of the $u = 0$ curve in figure 4 from $Z = 6{\cdot}565$ is only about twice the displacement of the point $u = 0$ from the minimum of v in the free viscous layer, shown in figure 13.

On increasing Z beyond the neighbourhood of Z_1, the viscous forces die out, and there is a repetition of the behaviour of u, v in the interval $0 < Z < Z_1$, except that $C^{(0)}$ and $A^{(0)}$ are now to be associated with $C^{(1)}$ and $A^{(1)}$. The process continues indefinitely with each viscous transition increasing the value of C

and A and also the minimum value of $-\psi$ and v. Thus, there is a modulation in the cycle of $r^n u$ versus $r^n v$, which presumably decays as $Z \to \infty$, in some sense, into the point $r^n u = 0$, $r^n v = 1$. A more detailed discussion of the decay will be given elsewhere.

The authors are grateful to the computer centre of The Ohio State University for making time available on the IBM 360/75 digital computer.

REFERENCES

ANDERSON, O. L. 1966 Numerical solutions of the compressible boundary-layer equations for rotating axisymmetric flows. Ph.D. thesis, Hartford Graduate Center, Rensselaer Polytechnic Institute.

BELCHER, R. 1970 The structure of a laminar boundary layer under a generalized vortex, Ph.D. thesis, Ohio State University.

BÖDEWADT, U. T. 1940 Die Drehströmung über festem Grunde. *Z. angew. Math. Mech.* **20**, 241.

BROWN, S. & STEWARTSON, K. 1969 Laminar separation. *Ann. Rev. Fluid Mech.* vol. 1.

BURGGRAF, O. R., STEWARTSON, K. & BELCHER, R. 1971 Boundary layer induced by a potential vortex. *Phys. Fluids*, **14**, 1821–1833.

COOKE, J. C. 1966 Numerical solution of Taylor's swirl atomizer problem. *R.A.E. Tech. Rep.* no. 66128.

CRANK, J. & NICHOLSON, P. 1947 A practical method for numerical evaluation of solutions of partial differential equations of the heat-conduction type. *Proc. Cam. Phil. Soc.* **43**, 50.

GOLDSHTIK, M. A. 1960 A paradoxical solution of the Navier–Stokes equations. *J. Appl. Math. Mech.* **24**, 913.

GOLDSTEIN, S. 1965 On backward boundary layers and flow in converging passages. *J. Fluid Mech.* **21**, 33.

HALL, M. G. 1969 The boundary layer over an impulsive started flat plate. *Proc. Roy. Soc.* A **310**, 401.

KENDALL, J. M. 1962 Experimental study of a compressible viscous vortex. *Jet Prop. Lab., Pasadena, Calif., Tech. Rep.* no. 32–290.

KING, W. S. & LEWELLEN, W. S. 1964 Boundary-layer similarity solutions for rotating flows with and without magnetic interaction. *Phys. Fluids*, **7**, 1674.

KUO, H. L. 1971 Axisymmetric flows in the boundary layer of a maintained vortex. *J. Atmos. Sci.* **28**, 20.

MCLEOD, J. B. 1971 The existence of axially symmetric flow above a rotating disk. *Proc. Roy. Soc.* A **324**, 391.

MACK, L. 1962 The laminar boundary layer on a disk of finite radius in a rotating flow. Part 1. *Jet Prop. Lab., Pasadena, Calif., Tech. Rep.* no. 32–224.

PEARSON, C. E. 1965 Numerical solutions for the time-dependent viscous flow between two rotating coaxial disks. *J. Fluid Mech.* **21**, 623.

RAYLEIGH, LORD 1916 On the dynamics of revolving fluids. *Proc. Roy. Soc.* A **93**, 148.

REYHNER, T. A. & FLÜGGE-LOTZ, I. 1968 The interaction of a shock wave with a laminar boundary layer. *Int. J. Non-lin. Mech.* **3**, 173.

RIEHL, H. 1954 *Tropical Meteorology*. McGraw-Hill.

ROTT, N. & LEWELLEN, W. S. 1966 Boundary layers and their interactions in rotating flows. In *Progress in Aeronautical Science* (ed. D. Küchemann), vol. 7, p. 111. Pergamon.

SCHLICHTING, H. 1968 *Boundary-Layer Theory* (6th edn.). McGraw-Hill.

SERRIN, J. 1972 The swirling vortex. *Phil. Trans. Roy. Soc.* A **270**, 325–360.

STEWARTSON, K. 1958 On rotating laminar boundary layers. *Boundary-Layer Research, Symp.*, Freiburg, p. 59. Springer.